

Figure 1. Description of the studied region. Panels a) and c) display the 4 nested domains used for the weather research and forecasting (WRF) simulation. Panel b) also includes the location of the Chacaltaya station (CHC, 5.2 km a.s.l.), La Paz City (LPB, 3.6 km a.s.l.) and Lake Titicaca (TCC, 3.9 km a.s.l.). Panels b) and d)

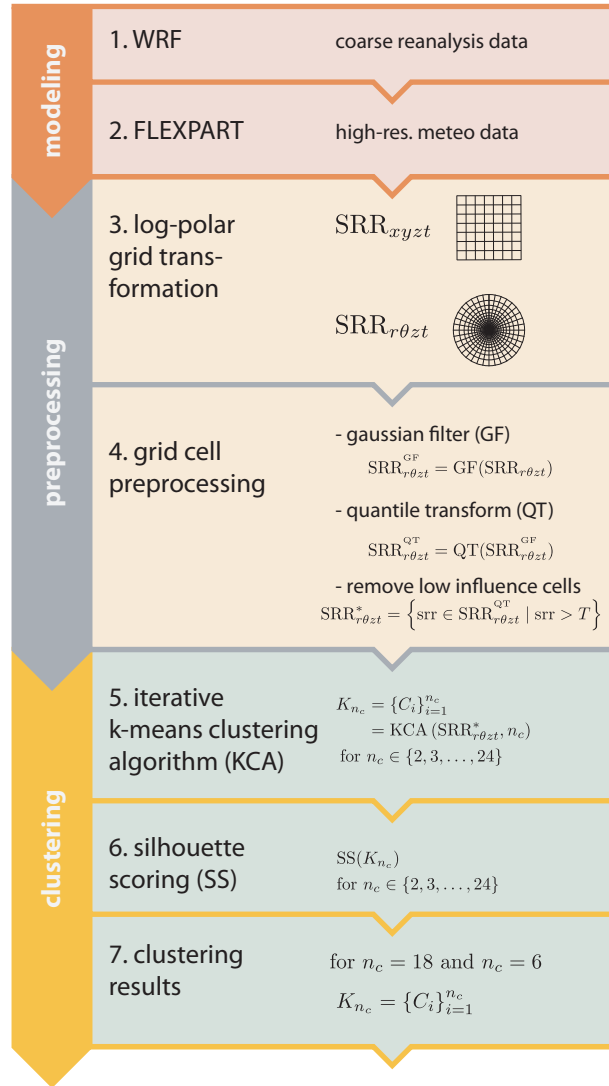


Figure 2. Flowchart describing the method's steps. The steps are divided in three groups: modeling, preprocessing and and clustering. SRR refers to the source

| | lower left [°] | | upper right [°] | | | number of cells | | parent start | |
|--------|----------------|-------|-----------------|-------|--------|-------------------|-------------------|--------------|-----|
| domain | lat. | lon. | lat. | lon. | p.g.r* | w.e. [†] | s.n. [‡] | i | j |
| D01 | -0.5 | -89.4 | -32.2 | -43.2 | 1 | 118 | 86 | 1 | 1 |
| D02 | -26.3 | -78.7 | -7.2 | -53.9 | 4 | 253 | 205 | 28 | 18 |
| D03 | -20.5 | -70.9 | -13.9 | -62.0 | 3 | 274 | 214 | 80 | 65 |
| D04 | -17.2 | -69.0 | -15.6 | -67.3 | 3 | 154 | 151 | 61 | 110 |

*parent grid ratio, [†]west east, [‡]south north

Table 1. Description of the domains used for the WRF simulation.

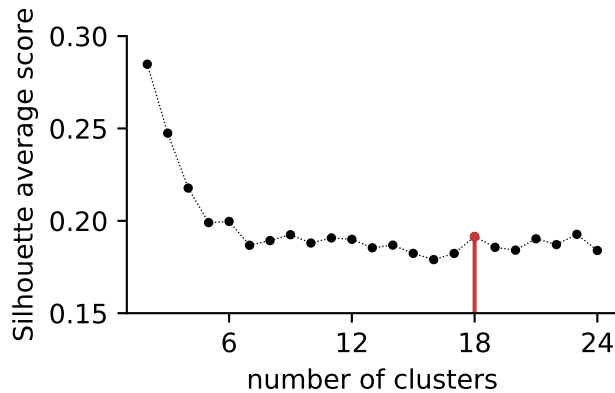


figure 3. Silhouette average score for the iterative ‘k means’ clustering algorithm from 2 to 24 number of clusters. We decide to use 18 clusters since it has a local

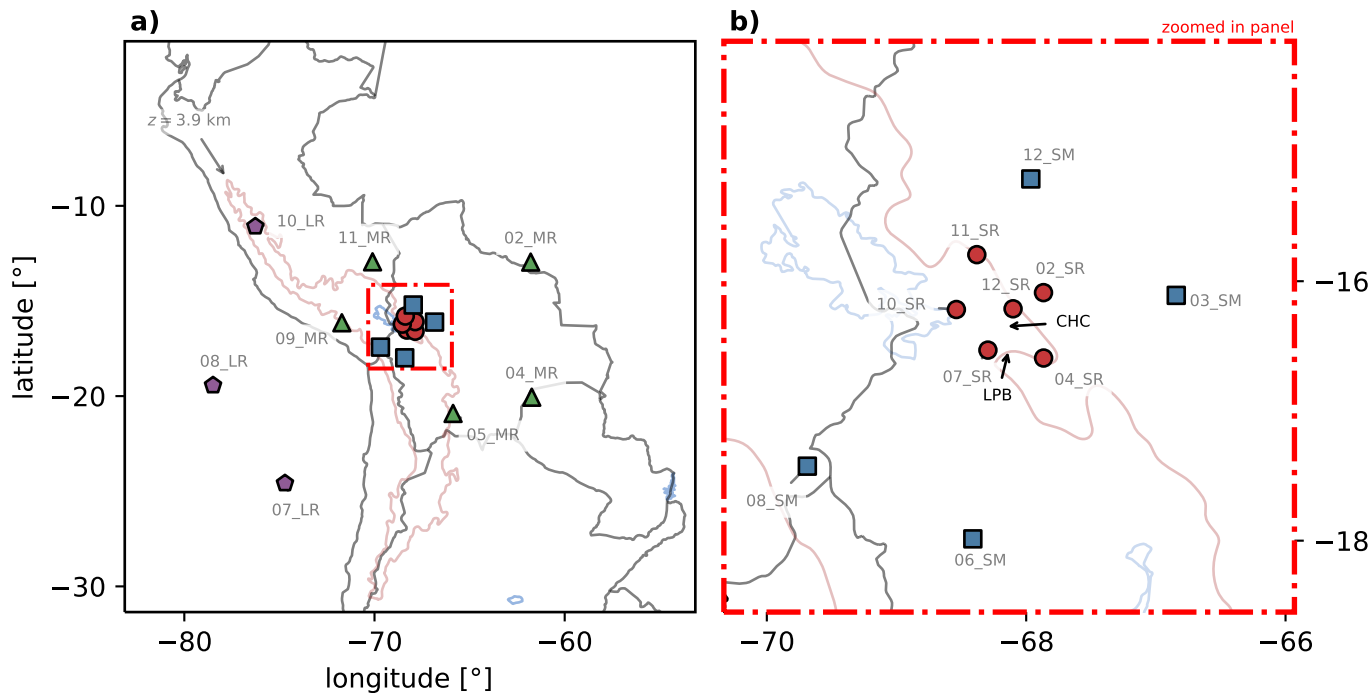


Figure 4. Horizontal center of mass of the 18 clusters. Each cluster centroid is marked with a disk (short range), square (short medium range), triangle (medium range), or pentagon (long range) locator. The brown line corresponds to a height of 3.9 km a.s.l. and encircles the Altiplano plateau. Panel b) corresponds to the region inside the red rectangle in panel a). The city of La Paz (panel b)) is located in the intersection of clusters 07_SR and 04_SR. The first cluster contains the part

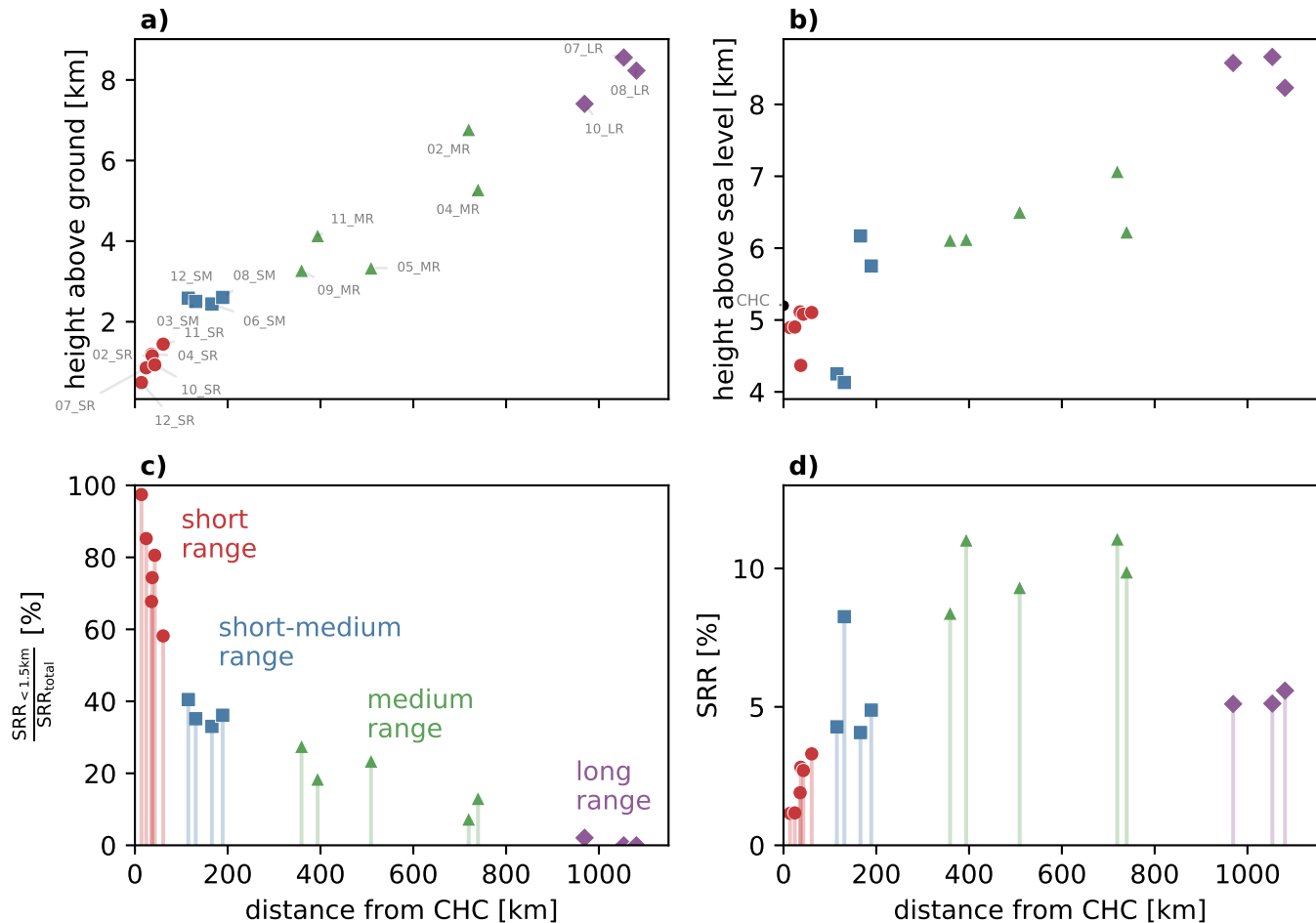


Figure 5. Cluster mean properties for each cluster. The horizontal axis for all panels represents the radial distance from CHC. Panel a) shows the median height above ground level of each cluster while panel b) portrays the height above sea level. Panel c) show the ratio between the SRR values that are below 1.5 km above ground

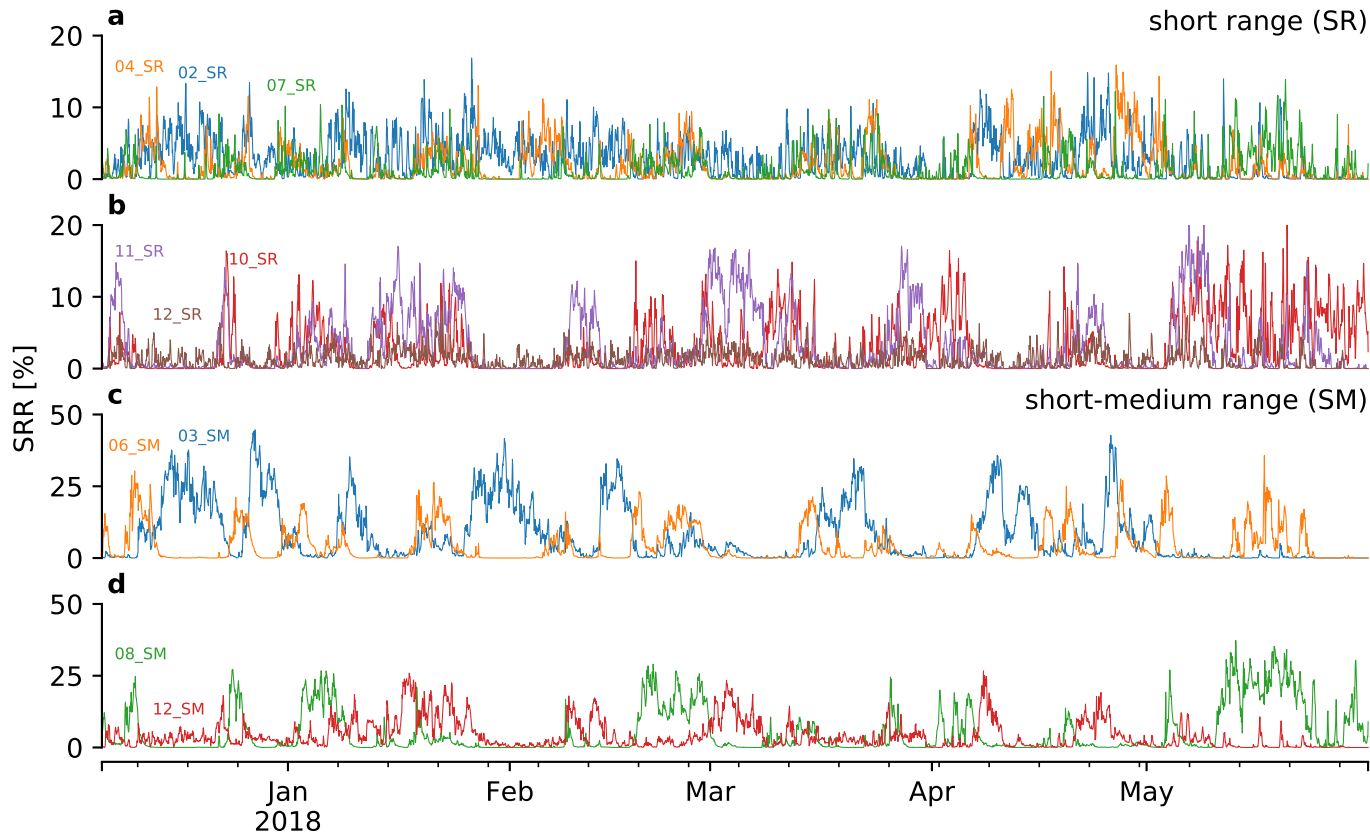


Figure 6. Time series of the SRR [%] cluster influence. Panels a and b show the short range (SR) clusters. Panels c and d display the short-medium range (SM)

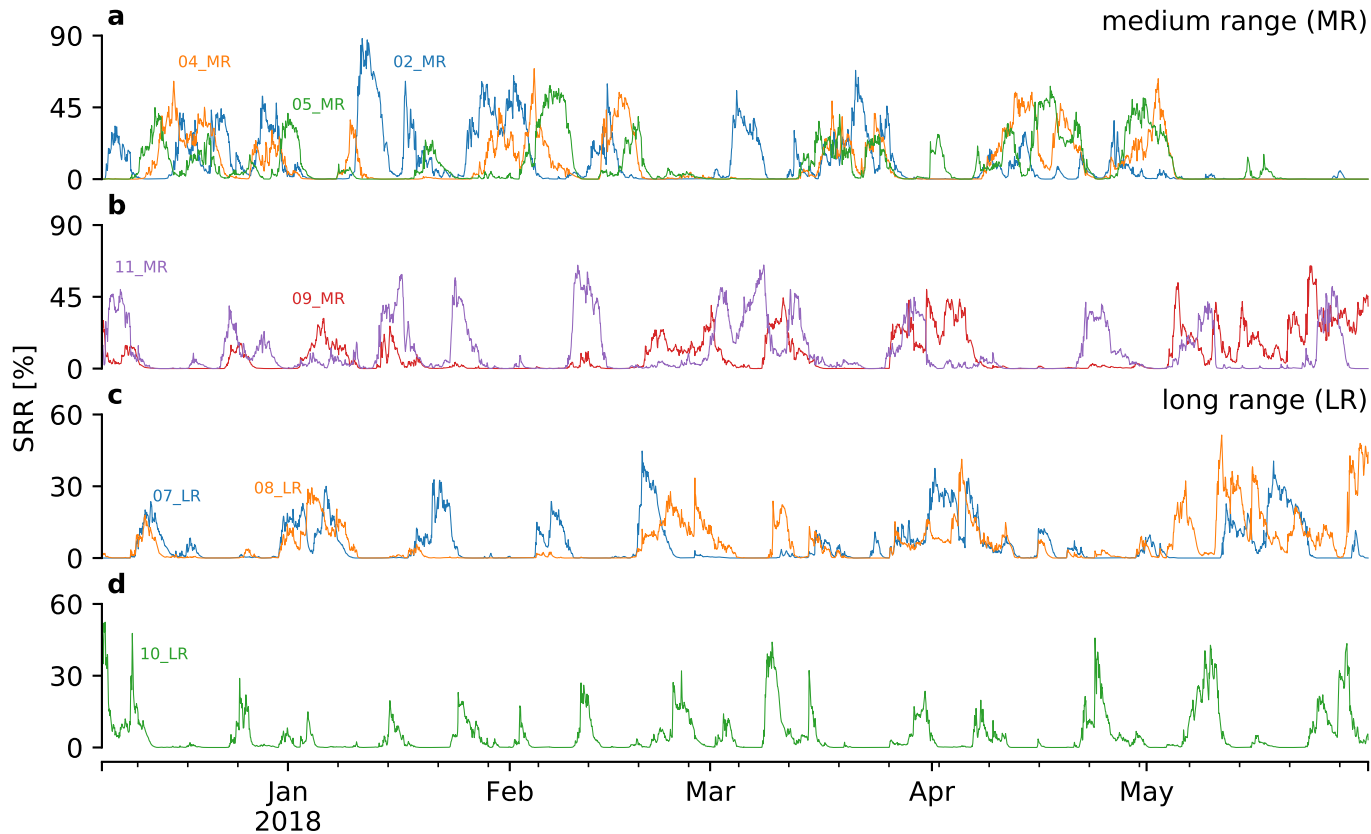


Figure 7. Time series of the SRR [%] cluster influence (similar to fig. 6). Panels a and b show the medium range (MR) clusters. Panels c and d display the long range

| | short name | SRR [%] $n_c = 18$ | distance from CHC [km] | height above ground [km] | height above sea level [km] | $\frac{\text{SRR}_{<1.5\text{km}}}{\text{SRR}_{\text{total}}} [\%]$ | main pathway | SRR [%] $n_c = 6$ |
|--|---------------|-----------------------|---------------------------|-----------------------------|--------------------------------|---|-----------------|----------------------|
| | 03_SM | 8.0 | 131 | 2.52 | 4.14 | 36 | 03_PW | 28.3 |
| | 02_MR | 10.7 | 713 | 6.83 | 7.13 | 7 | | |
| | 04_MR | 9.6 | 728 | 5.28 | 6.23 | 14 | | |
| | 04_SR | 1.9 | 36 | 1.24 | 5.14 | 68 | 05_PW | 11.1 |
| | 05_MR | 9.2 | 509 | 3.35 | 6.51 | 24 | | |
| | 06_SM | 4.1 | 165 | 2.38 | 6.13 | 34 | 07_PW | 15.6 |
| | 07_LR | 5.5 | 1045 | 8.55 | 8.66 | 0 | | |
| | 08_LR | 6.1 | 1080 | 8.23 | 8.23 | 0 | | |
| | 07_SR | 1.2 | 24 | 0.83 | 4.87 | 85 | 08_PW | 17.9 |
| | 10_SR | 2.8 | 43 | 0.91 | 5.04 | 81 | | |
| | 08_SM | 5.2 | 189 | 2.55 | 5.73 | 38 | | |
| | 09_MR | 8.8 | 359 | 3.27 | 6.11 | 29 | | |
| | 11_SR | 3.2 | 61 | 1.45 | 5.10 | 59 | 11_PW | 19.0 |
| | 11_MR | 10.7 | 392 | 4.15 | 6.12 | 19 | | |
| | 10_LR | 5.0 | 950 | 7.48 | 8.66 | 2 | | |
| | 12_SR | 1.2 | 14 | 0.53 | 4.90 | 98 | 12_PW | 8.1 |
| | 02_SR | 2.8 | 37 | 1.18 | 4.38 | 75 | | |
| | 12_SM | 4.1 | 116 | 2.61 | 4.25 | 42 | | |

Table 2. Describes the properties of the eighteen clusters ($n_c = 18$). The short-name’s digits refer to the clockwise direction of the center of mass of each cluster. The letters refer to the range: SR = short range, SM = short medium range, MR = medium range, and LR = long range. The SRR [%] column describe the average contribution of each cluster. We also show the distance from CHC, height above ground and height above sea level of each cluster’s center of mass. Furthermore, $\frac{\text{SRR}_{<1.5\text{km}}}{\text{SRR}_{\text{total}}} [\%]$ shows the ratio between the SRR below 1.5 km and the SRR summed over the full vertical column ($\text{SRR}_{\text{total}}$). The last two columns describe the results of clustering the 18 clusters into 6 clusters (main pathways, $n_c = 6$). The digits also refer to the clockwise direction. Finally the last columns adds up the SRR [%] of the cluster belonging to each main pathway.

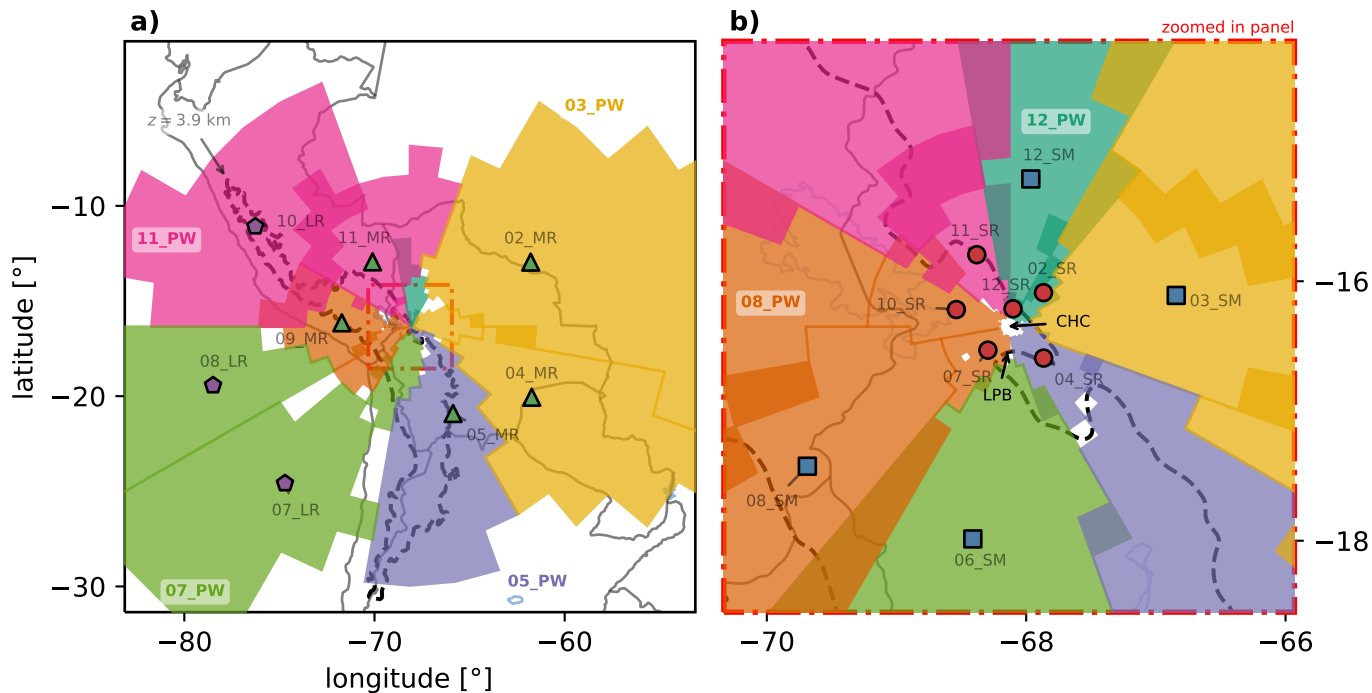


Figure 8. Similar to fig. 4 including the horizontal location of the 18 clusters but also adding the main 6 pathways (PW). Each cluster centroid is marked with a disk (circle (short range), square (short medium range), triangle (medium range), or pentagon (long range) locator. For each cluster we select cells that contain 80% of its SRR values during the modeling period. The color of each cluster is related to the main pathway they belong to: 03_PW (yellow), 05_PW (purple), 07_PW (green), 08_PW (orange), 11_PW (pink), and 12_PW (teal). Cluster boundaries are delimited by a darker ‘border’ line. The dashed black line corresponds to a height of 3.9 km a.s.l. and encircles the Altiplano plateau. Panel b) corresponds to the region inside the red rectangle in panel a). The city of La Paz (panel b)) is located in the intersection

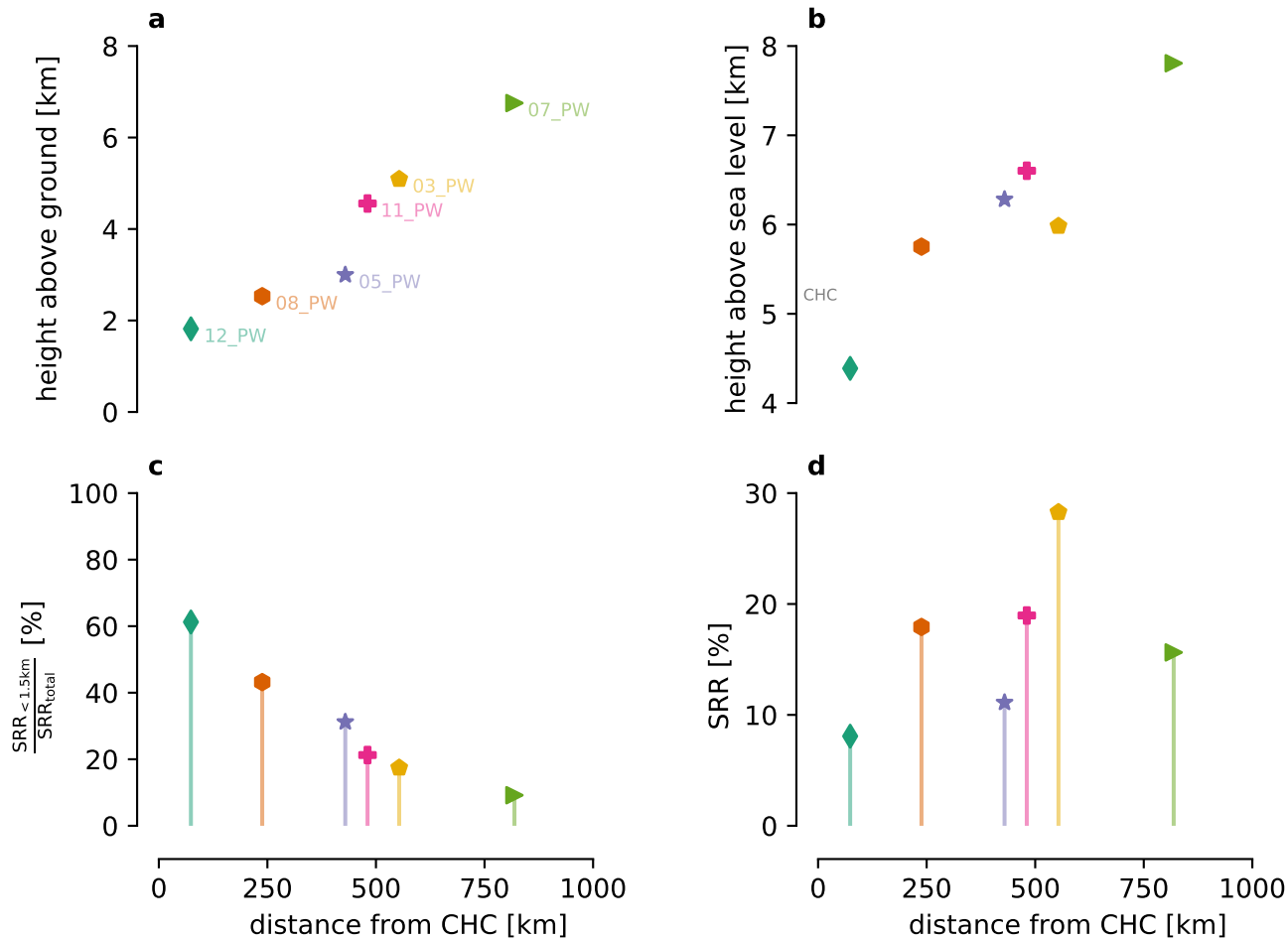


Figure 9. Centroid properties for each of the main pathways (PW). This figure is similar to fig. 5. Panel a shows the median height above ground level of each cluster while panel b portrays the height above sea level. Panel c shows the ratio between the SRR values that are below 1.5 km above ground level and the total SRR value

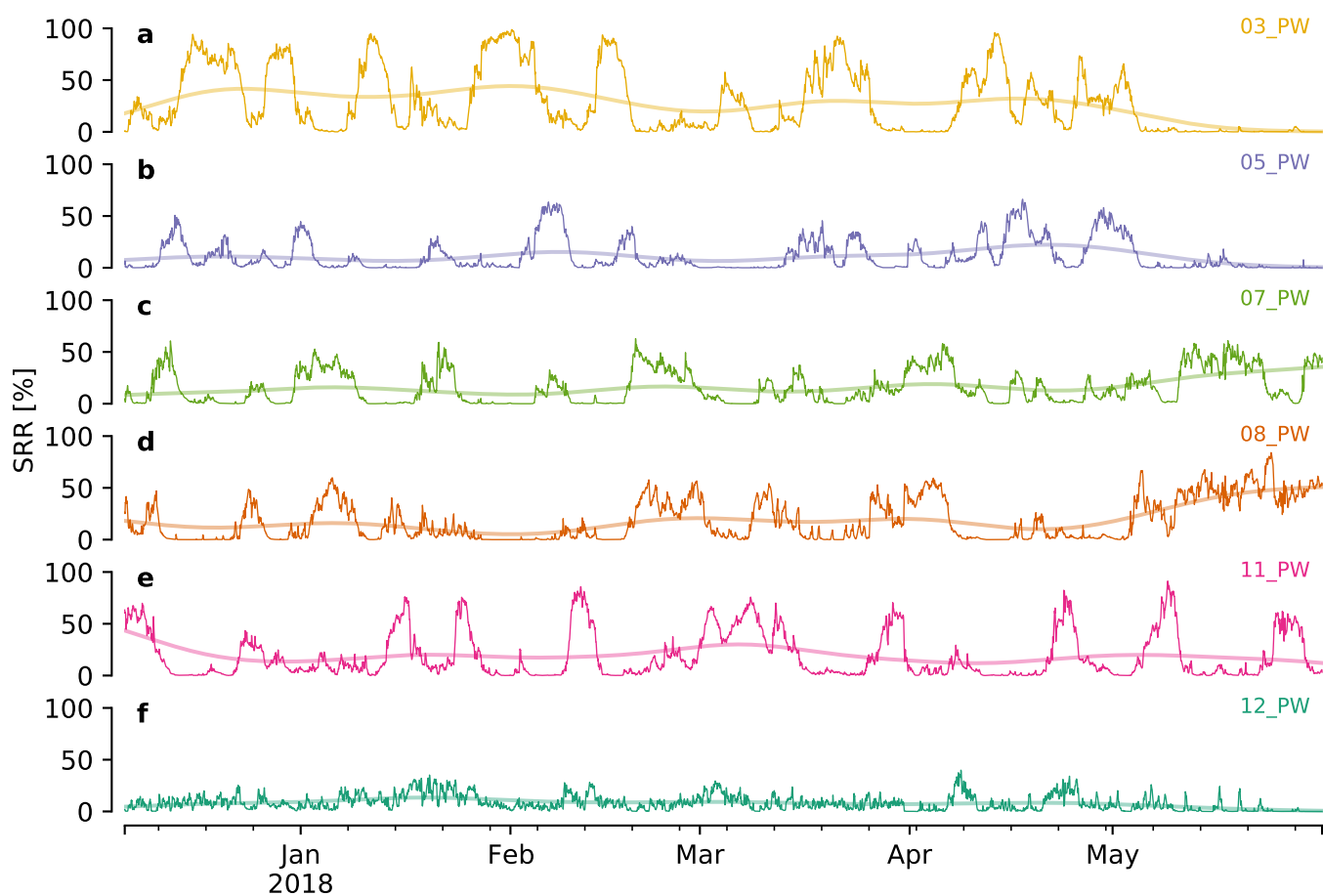


Figure 10. Time series of the SRR [%] influence for each main pathway (PW). The figure is similar to figs. 6 and 7. The smooth line on each panel is obtained by applying a gaussian filter on the original dataset with $\text{std}=10$ days. It can be seen that 03_PW, 05_PW and to a lesser extent 12_PW reduce their influence in May which is the transition month between the wet and the dry season suggesting that these pathways are more influential during the wet season. 07_PW and 08_PW

| | main pathway | SRR [%] $n_c = 6$ | distance from CHC [km] | height above ground [km] | height above sea level [km] | $\frac{\text{SRR}_{<1.5\text{km}}}{\text{SRR}_{\text{total}}} [\%]$ |
|--|-----------------|----------------------|---------------------------|-----------------------------|--------------------------------|---|
| | 03_PW | 28.3 | 554 | 5.09 | 5.98 | 17 |
| | 05_PW | 11.1 | 429 | 3.00 | 6.28 | 31 |
| | 07_PW | 15.6 | 819 | 6.75 | 7.81 | 9 |
| | 08_PW | 17.9 | 238 | 2.53 | 5.75 | 43 |
| | 11_PW | 19.0 | 481 | 4.56 | 6.60 | 21 |
| | 12_PW | 8.1 | 74 | 1.82 | 4.39 | 61 |

Table 3. Describes the properties of the main 6 pathways (similar to table 2). The main-pathway's digits refer to the clockwise direction of the center of mass of the cluster masses. The colors are unique for each PW and the same scheme is used on table 2 and fig. 8. The SRR [%] columns describe the average contribution of each cluster. We also show the distance from CHC, height above ground and height above sea level of each cluster's center of mass. Furthermore, $\frac{\text{SRR}_{<1.5\text{km}}}{\text{SRR}_{\text{total}}} [\%]$ shows the ratio between the SRR below 1.5 km and the SRR summed over the full vertical column ($\text{SRR}_{\text{total}}$).

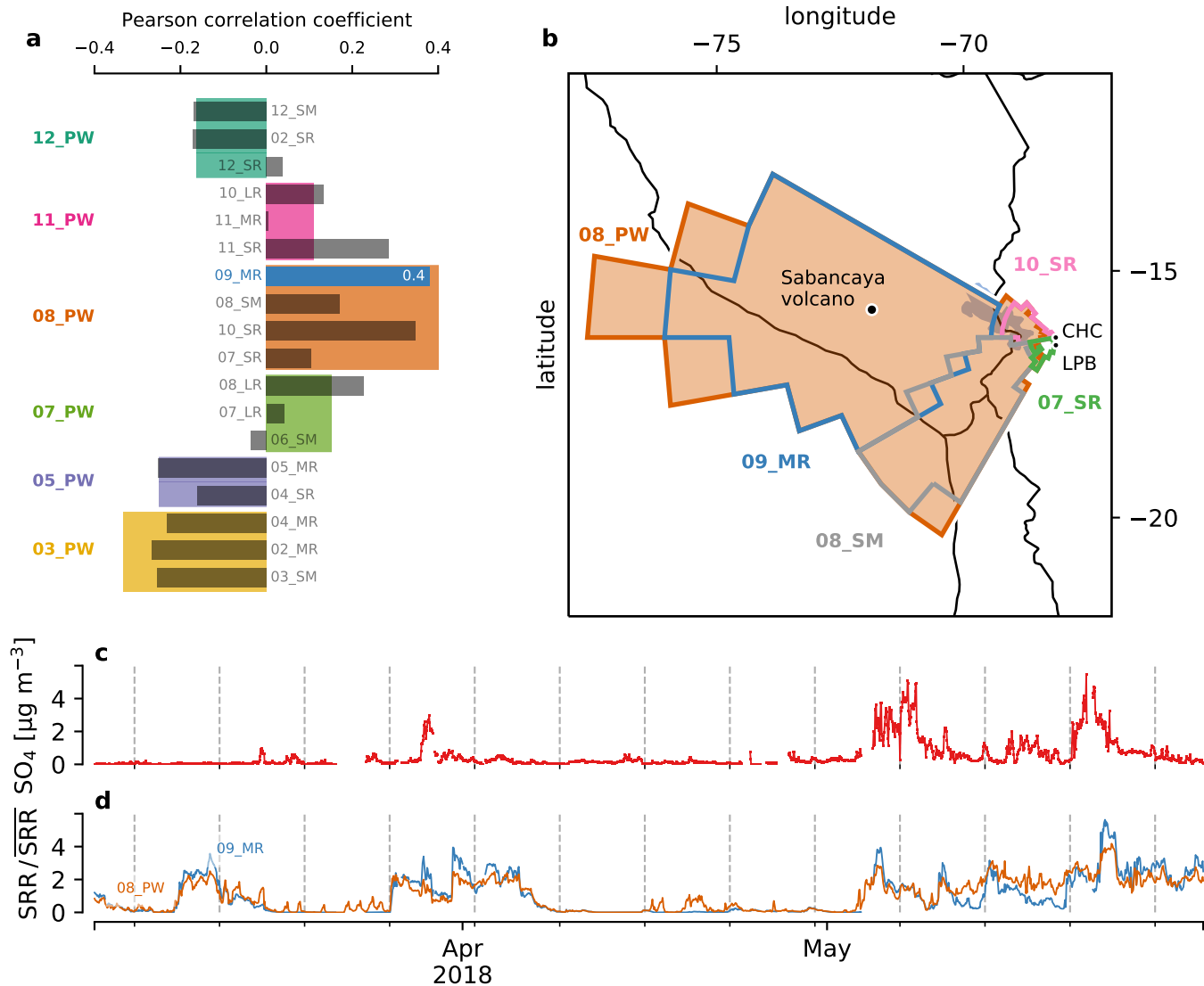


Figure 11. In panel a, we show the pearson correlation between SO_4 concentrations sampled at CHC and, both, the 18 clusters and the 6 pathways (PW). In panel b, the regions covered by the pathway 08_PW and the clusters 09_MR, 08_SM, 10_SR and 07_SR are shown. All of the aforementioned clusters are contained by